

Penning-Trap Mass Measurements in Atomic and Nuclear Physics

Jens Dilling,^{1,2} Klaus Blaum,³ Maxime Brodeur,⁴
and Sergey Eliseev³

¹TRIUMF, Vancouver, British Columbia V6T 2A3, Canada

²Department of Physics and Astronomy, University of British Columbia, Vancouver, British Columbia V6T 1Z1, Canada

³Max-Planck-Institut für Kernphysik, 69117 Heidelberg, Germany

⁴Department of Physics, University of Notre Dame, Notre Dame, Indiana 46556, USA

Annu. Rev. Nucl. Part. Sci. 2018. 68:45–74

First published as a Review in Advance on
May 23, 2018

The *Annual Review of Nuclear and Particle Science*
is online at nucl.annualreviews.org

<https://doi.org/10.1146/annurev-nucl-102711-094939>

Copyright © 2018 by Annual Reviews.
All rights reserved

**ANNUAL
REVIEWS CONNECT**

www.annualreviews.org

- Download figures
- Navigate cited references
- Keyword search
- Explore related articles
- Share via email or social media

Keywords

ion trap, single-ion spectroscopy, online mass measurements, fundamental symmetries, neutrinos, nuclear halos

Abstract

Penning-trap mass spectrometry in atomic and nuclear physics has become a well-established and reliable tool for the determination of atomic masses. In combination with short-lived radioactive nuclides it was first introduced at ISOLTRAP at the Isotope Mass Separator On-Line facility (ISOLDE) at CERN. Penning traps have found new applications in coupling to other production mechanisms, such as in-flight production and separation systems. The applications in atomic and nuclear physics range from nuclear structure studies and related precision tests of theoretical approaches to description of the strong interaction to tests of the electroweak Standard Model, quantum electrodynamics and neutrino physics, and applications in nuclear astrophysics. The success of Penning-trap mass spectrometry is due to its precision and accuracy, even for low ion intensities (i.e., low production yields), as well as its very fast measurement cycle, enabling access to short-lived isotopes. The current reach in relative mass precision goes beyond $\delta m/m = 10^{-8}$, the half-life limit is as low as a few milliseconds, and the sensitivity is on the order of one ion per minute in the trap. We provide a comprehensive overview of the techniques and applications of Penning-trap mass spectrometry in nuclear and atomic physics.

Contents

1. INTRODUCTION	46
2. FUNDAMENTAL PRINCIPLE OF PENNING TRAPS	47
2.1. Ion Motion in a Penning Trap	47
2.2. Techniques for Measuring the Cyclotron Frequency	48
3. FACILITY OVERVIEW: PENNING-TRAP MASS SPECTROMETERS	52
3.1. Penning-Trap Mass Measurements of Unstable Isotopes	53
3.2. Penning-Trap Mass Measurements of Stable Isotopes	57
4. NUCLEAR PHYSICS APPLICATIONS	59
4.1. Mass Measurements for Nuclear Structure Studies	59
4.2. Mass Measurements for Nuclear Astrophysics Studies	62
5. MASS MEASUREMENTS FOR FUNDAMENTAL PHYSICS TESTS	63
5.1. Mass Measurements for Neutrino Physics Studies	63
5.2. Test of the Standard Model via Weak Interaction Studies	67
5.3. Masses of the Lightest Particles	67
6. CONCLUSION AND OUTLOOK	69

1. INTRODUCTION

The mass of an atom or a nucleus is unique, like the fingerprint of a human being, as it allows the atom or nucleus to be unambiguously identified. Atomic masses also provide insight into the nucleus's state (i.e., whether it is in the ground state or a low-lying isomeric state) while providing access to the binding energies of the fundamental building blocks of the atom: protons, neutrons, and electrons. Since the birth of mass spectrometry with Thomson's (1) discovery of the existence of neon isotopes in 1913, more refined mass spectrometry methods have been invented (2). The most modern mass spectrometry method that provides the highest mass precision and mass-resolving power relies on the measurement of the oscillation frequency with which an ion of interest revolves in a magnetic field. The device of choice that enables the confinement of ions is the Penning trap, which currently offers relative mass uncertainties down to 10^{-10} for radionuclides (3, 4) and even below 10^{-11} for stable species (5). Along with improvements in precision, efficiency, and resolution, the application to species with an ever greater neutron-to-proton imbalance has expanded, along with the range of applications. As a result, detailed information on the binding energies of more than 3,000 species throughout the chart of nuclides, including radionuclides at extreme proton-to-neutron ratios, is available. New mass data, in particular of nuclides far from stability with relative mass uncertainties of 10^{-6} and below, provide indispensable nuclear physics input for astrophysical models and, thus, for our understanding of the processes of element formation in the Universe. Direct mass difference (Q value) measurements of specific isotopes play a key role in neutrino physics research. Furthermore, the mass determination of elementary particles, such as electrons or protons, represents an important part of our system of fundamental constants. For the latter, relative mass uncertainties at the 10^{-11} level are required. Finally, attempts are under way to replace the present macroscopic standard for the mass unit by an atomic standard, which is expected to take effect in 2019.

This article reviews the fundamental principles of Penning traps (Section 2), including novel ion manipulation, cooling, and detection techniques, and provides a detailed overview of all high-precision Penning-trap mass spectrometers installed at radioactive ion beam (RIB) facilities, as well as offline installations for stable and long-lived species (Section 3). In Sections 4 and 5, we

discuss applications of high-precision mass data in nuclear physics as well as fundamental physics research.

2. FUNDAMENTAL PRINCIPLE OF PENNING TRAPS

2.1. Ion Motion in a Penning Trap

The Penning trap is a superposition of a static strong uniform magnetic field B and a static three-dimensional quadrupolar electric potential $U(r, z)$:

$$U(r, z) = \frac{U_0}{4d^2}(2z^2 - r^2). \quad 1.$$

Here, d is the characteristic dimension of the Penning trap; U_0 is the potential difference between adjacent trap electrodes (trapping voltage); and r and z are the radial and axial coordinates, respectively, with respect to the center of the trap. Such a quadrupolar electric potential is created by means of two electrodes shaped like infinite hyperboloids of revolution. In practice, a reasonably quadratic electric potential in the ion trapping region is produced with either (a) two finite hyperboloids of revolution and two additional correction electrodes or (b) a stack of several (usually five) cylindrical electrodes.

The fields are oriented in such a way that an electrostatic potential well is created along the magnetic field lines. In such a configuration, the magnetic field confines the ion motion to the plane perpendicular to the magnetic field lines (radial motions), whereas the electrostatic potential well traps ions along the magnetic field lines (axial motion) (**Figure 1**). The detailed theory of the Penning trap can be found in, for example, Reference 6.

The determination of the mass m of an ion with electric charge q in a Penning trap is based on the measurement of its cyclotron frequency ν_c (the frequency of the ion motion in a pure magnetic field):

$$\nu_c = \frac{1}{2\pi} \cdot \frac{q}{m} \cdot B. \quad 2.$$

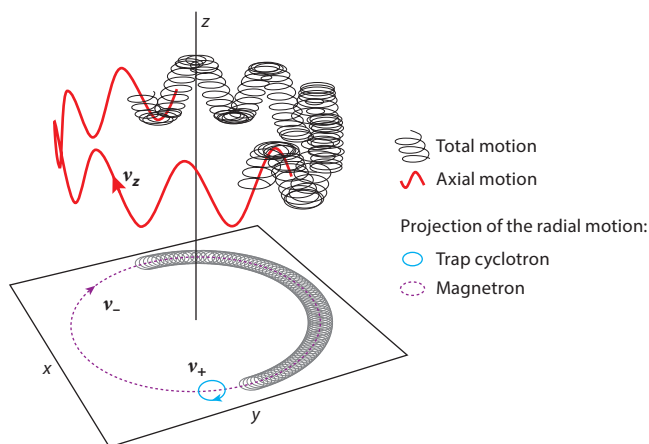


Figure 1

An illustration of the ion motion in a Penning trap. In the z direction, the ion performs periodic oscillations in the trap electrostatic potential with frequency ν_z . In the radial plane (xy plane), the ion performs two trap motions: fast cyclotron motion with frequency ν_+ and slow magnetron motion ν_- . A superposition of these motions creates a complex trajectory of the ion motion (black line).

The presence of the electrostatic quadrupolar field modifies the cyclotron motion of an ion in the magnetic field and results in three independent trap eigenmotions with frequencies (**Figure 1**)

$$\nu_+ = \frac{\nu_c}{2} + \sqrt{\frac{\nu_c^2}{4} - \frac{\nu_z^2}{2}} - \text{modified cyclotron motion}, \quad 3.$$

$$\nu_- = \frac{\nu_c}{2} - \sqrt{\frac{\nu_c^2}{4} - \frac{\nu_z^2}{2}} - \text{magnetron motion}, \quad 4.$$

$$\nu_z = \frac{1}{2\pi} \sqrt{\frac{qU}{md^2}} = \frac{1}{2\pi} \sqrt{c_2 U} - \text{axial motion}. \quad 5.$$

The magnetron motion is simply an $\mathbf{E} \times \mathbf{B}$ drift motion. The frequency hierarchy is $\nu_c > \nu_+ \gg \nu_z \gg \nu_-$ for typical trap parameters and ion masses.

The ion mass is determined from the invariance theorem, which links the eigenfrequencies to the cyclotron frequency as follows (7):

$$\nu_c^2 = \nu_+^2 + \nu_-^2 + \nu_z^2. \quad 6.$$

This relation is applicable not only to an ideal Penning trap but also to existing Penning-trap systems with small imperfections in the alignment of the electric and magnetic fields (7).

In high-precision Penning-trap mass spectrometry of short-lived nuclides, a simpler relation of the cyclotron frequency to the trap eigenfrequencies is employed:

$$\nu_c = \nu_+ + \nu_-. \quad 7.$$

This relation enables determination of the mass ratio of two ions with similar masses with a relative uncertainty down to at least few parts in 10^{10} for all existing online Penning-trap facilities (8).

2.2. Techniques for Measuring the Cyclotron Frequency

High-precision Penning traps naturally fall into two groups: (a) online facilities for mass measurements on short-lived nuclides with typical relative uncertainties down to 10^{-8} for nuclear physics (9–16) and (b) offline setups for measuring mass ratios of long-lived or stable nuclides with relative uncertainties well below 10^{-10} for fundamental physics (17–21). It is not surprising that such different types of Penning-trap facilities employ very different techniques to measure the cyclotron frequency.

At online facilities, the time-of-flight ion cyclotron resonance (ToF-ICR) (22) technique was until recently the method of choice due to its speed, relative simplicity, and sensitivity to a single ion in the trap at room temperature. The drawback of this technique is that it is destructive; thus, at least a few hundred ions are required to reach a sufficiently low uncertainty in mass determination. Recently, the novel phase-image ion cyclotron resonance (PI-ICR) (23) technique was developed at SHIPTRAP. Its goal is to replace the ToF-ICR technique in mass measurements on very short-lived nuclides and low-lying nuclear isomeric states.

In cryogenic offline setups, the fast Fourier ion cyclotron resonance (FT-ICR) (24) technique is employed. This method enables frequency measurements on a single ion with an extraordinary low uncertainty. The trade-off is the high complexity of the system, which requires that both the trap and the associated frequency measurement electronics be cooled to the temperature of liquid helium.

2.2.1. Time-of-flight ion cyclotron resonance. Until now, masses of short-lived nuclides with Penning traps have been determined by extracting an ion from the Penning trap and measuring its ToF through the strong gradient of a magnetic field. The ToF of an ion in the z direction between the trap located at the zero position and the detector at z_{det} , placed onto the trap axis in the region with a weak magnetic field, is a function of the ion orbital magnetic moment $|\mu| = |E_r/B_0|$ in the Penning trap and is given by

$$T(E_r) = \int_0^{z_{\text{det}}} dz \cdot \sqrt{\frac{m}{2(E_0 - qU(z) + |\mu(E_r)B(z)|)}}, \quad 8.$$

where E_r is the ion radial kinetic energy; B_0 is the magnetic field at the trap center; E_0 is the total initial axial energy of the ion; and $U(z)$ and $B(z)$ are the electric potential and magnetic field, respectively, along the ion path between the trap and detector.

The orbital magnetic moment of the ion in the trap, and hence its ToF to the detector, can be manipulated by applying a multipolar radio-frequency (rf) field at a frequency near $n\nu_c$, where $n = 1$ and $n = 2$, for example, correspond to quadrupolar and octupolar rf fields, respectively. By varying the frequency and keeping constant the amplitude and duration of this rf excitation, one obtains the ToF versus frequency of the rf field, known as the ToF resonance.

In practice, until recently only the quadrupolar rf excitation ($n = 1$) was routinely used to measure the cyclotron frequency, since only for this multipolarity can the shape of the ToF resonance be calculated analytically (25). From the invention of this technique in 1980 (22) until approximately 2007, the only temporal profile of the rf excitation was a single constant-amplitude rf pulse of duration t . Such a temporal rf pulse results in a ToF resonance with a single pronounced minimum and a series of smaller minima on both sides (**Figure 2a**). In 1992, researchers pointed out (26) that an alternative profile of the rf pulse, namely a sequence of two short rf pulses separated by a long interval, should enable a more precise measurement of the cyclotron frequency, since the corresponding ToF resonance has several almost equally pronounced minima (fringes), rather than one (**Figure 2b**). The practical realization of what would become known as the Ramsey technique had to wait until 2007, when a detailed analytical description of this excitation scheme was proposed (27–29). Since then, this excitation pattern of time-separated oscillatory fields has been the method of choice for the majority of mass measurements using the ToF-ICR technique.

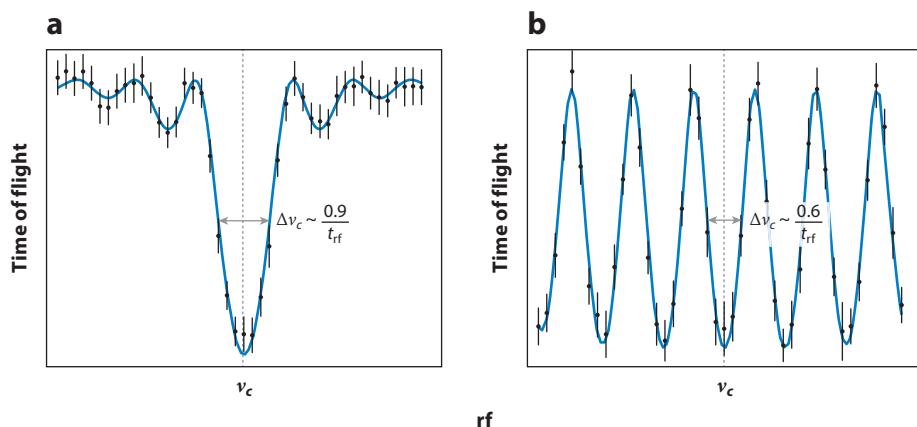


Figure 2

The line shape of the time of flight using (a) a one-pulse radio-frequency (rf) field and (b) a two-pulse rf field of total duration t .

Further progress in developing the mass-resolving power and precision of the ToF-ICR technique can be achieved through the implementation of excitation rf fields of higher multiplicities, primarily the octupolar rf field. Early attempts to experimentally implement the ToF-ICR technique with the octupolar rf field were undertaken in 2007 at LEBIT and SHIPTRAP (30, 31). These experiments showed that the use of one-pulse rf field of carefully chosen amplitude and duration results in a very narrow ToF resonance, and demonstrated a gain in resolving power of one order of magnitude (31).

The only successful application of the ToF-ICR technique with octupolar rf pulse to mass measurements was demonstrated at SHIPTRAP in the determination of the Q value of the double electron capture (EC) in ^{164}Er (32). This experiment measured the ratio of the cyclotron frequencies of singly charged ^{164}Er and ^{164}Dy ions.

Although the ToF-ICR technique with the octupolar rf pulse has the potential for further development, the recently introduced PI-ICR technique (23) may make ToF-ICR obsolete.

2.2.2. Phase-image ion cyclotron resonance. The PI-ICR technique is based on the determination of $\nu_c = \nu_- + \nu_+$ through measurement of the phases of the ion magnetron and trap cyclotron motions (i.e., radial motions) in the trap after a given period of excitation-free propagation. After an ion is captured in the center of the Penning trap, its radial motion is excited to a certain initial radius and phase via a dipolar rf field at the radial-motion frequency. After free evolution for a given time t , the ion performs n revolutions and the radial ion motion accumulates a phase ϕ_{total} . The radial ion frequency ν is

$$\nu = \frac{\phi_{\text{total}}}{2\pi t}, \quad 9.$$

and the resolving power $\nu/\Delta\nu$ of the PI-ICR technique is given by

$$\frac{\nu}{\Delta\nu} \approx \pi n \frac{r}{\Delta r}, \quad 10.$$

where Δr is the initial half-width of the ion spatial distribution in the center of the trap.

Thus, in contrast to the resolving power of the ToF-ICR method, the resolving power of the PI-ICR technique does not depend only on the time the ions spend in the Penning trap. Rather, it can be substantially increased by bringing the ions onto a larger radius or by reducing the initial spatial distribution of the ions in the Penning trap.

In order to determine the accumulated phase ϕ_{total} , the ion motion is projected onto a position-sensitive MCP detector, which is placed on the Penning-trap axis in a weak magnetic field of a few milliTesla (**Figure 3**). A detailed description of the technique can be found in Reference 33. Compared with the ToF-ICR method, the PI-ICR technique offers an approximately fivefold gain in precision of the cyclotron-frequency determination and a 40-fold gain in resolving power under typical experimental conditions.

2.2.3. Fast Fourier ion cyclotron resonance. If the mass of a nuclide of interest is to be measured with a relative uncertainty well below 10^{-10} , ToF-ICR and PI-ICR become inapplicable. Instead, a set of techniques collectively known as FT-ICR are employed. These nondestructive techniques are based on a determination of the frequency of ion trap motion in that they measure the frequency of the current induced by the ion trap motion in a resonant circuit attached to corresponding trap electrodes (**Figure 4a**). The induced current is converted to a measurable voltage by means of a resonant inductor–capacitor (LC) circuit with a very high quality factor Q . Together with the circuit’s parasitic self-capacitance and the trap capacitance, the inductance forms a parallel resonant LC circuit (i.e., a resonator). The value of the inductance is chosen such

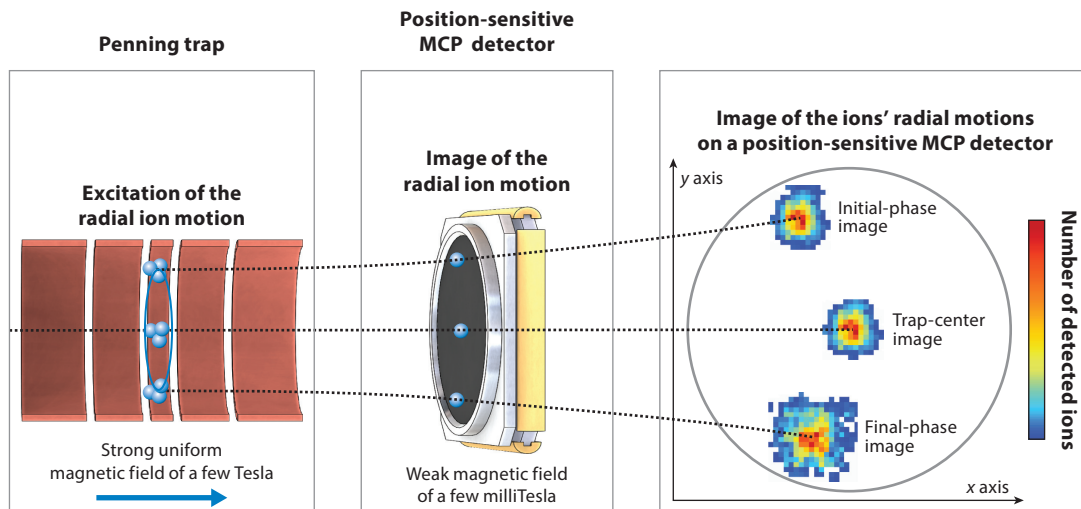


Figure 3

Illustration of the ion radial-motion projection onto a position-sensitive detector. Abbreviation: MCP, microchannel plate.

that the resonant frequency of the resonator is approximately equal to that of the ion motion. The resonator is usually connected to a low-noise voltage amplifier, which defines the signal-to-noise ratio of the induced-current frequency measurement system and decouples the resonator from the following signal-transfer line. The noise-density frequency spectrum of such an induced-current frequency measurement system without an ion in the trap has a typical peak shape at a resonant frequency $\nu_{LC} = 1/(2\pi\sqrt{LC_{\text{total}}})$ (**Figure 4a**). In order to provide a sufficiently high signal-to-noise ratio and sensitivity to a single ion in the trap, the electrodes of the Penning trap, together with the resonators and amplifiers, have to be operated at the temperature of liquid helium (approximately 4.2 K) and the ions have to be highly charged. These properties distinguish Penning-trap mass spectrometers based on the FT-ICR method from those based on the ToF-ICR or PI-ICR technique. The latter are usually operated at room temperature.

The ion that performs a coherent periodic motion in the trap with a frequency close to that of the resonator shows up in the noise-density frequency spectrum as a peak at the ion-motion frequency (**Figure 4b**). The height of the peak is proportional to the amplitude of the ion motion.

The resonator has a certain impact on the ion motion in the trap. From one side, the voltage induced on the electrodes creates an electric field across the trap that slows down the ion and, in general, changes its motion frequency. From the other side, the thermal noise of the resonator excites the ion motion. Thus, after awhile the ion motion comes into thermal equilibrium with the resonator. The noise-density frequency spectrum with a thermalized ion has a pronounced minimum (dip) at the frequency of the ion motion (**Figure 4c**) (34).

Usually, the axial motion of an ion is cooled directly through its coupling to a resonator with a resonant frequency close to the axial-motion frequency, whereas the radial motions are cooled indirectly through their coupling to the axial motion via an rf pulse at a certain frequency (35, 36). This is the most convenient way to cool the ion trap motion, since the frequency of the axial ion motion can easily be adjusted to the frequency of the resonator by varying the trap electric potential. The amplitudes of the ion trap motions that are brought into equilibrium with the axial resonator in this manner at a temperature of approximately 4.2 K do not exceed a few micrometers.

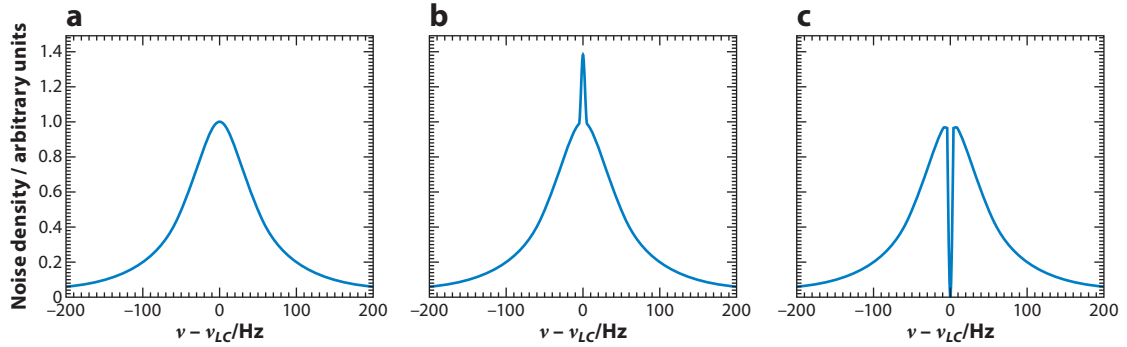
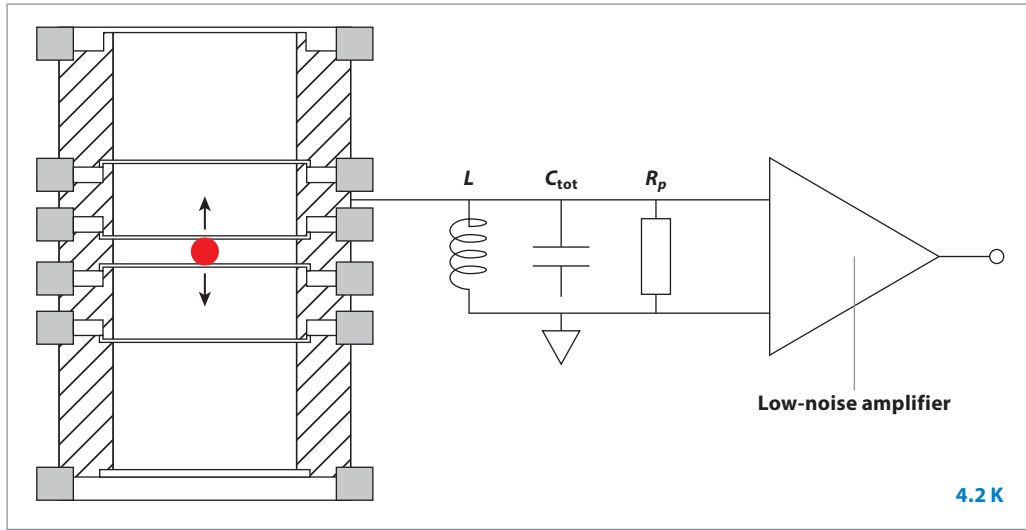


Figure 4

(Top) Resonant LC circuit for the measurement of the frequency of the image current induced by a moving charged particle. It is formed by an inductance L , which is connected to one of the trap electrodes, by a capacitance C_{total} being a product of parasitic self-capacitance of the inductance and the trap capacitance. The system also has a nonzero parasitic active resistance R_p . The resonant circuit is connected to a low-noise amplifier for amplifying the converted voltage and for decoupling the LC circuit for the following signal-transfer line. (a) A noise-density frequency spectrum of a resonant LC circuit without an ion in the trap. (b) The ion that performs a coherent periodic motion in the trap with a frequency close to that of the resonator shows up in the noise-density frequency spectrum as a peak at the ion-motion frequency. (c) A noise-density frequency spectrum of a resonant LC circuit with a thermalized ion in the trap.

The frequencies of the axial and magnetron motions are measured with the double-dip method (35, 36). By contrast, the phase-sensitive PnP/PnA (pulse and phase/pulse and amplify) method is used to measure the frequency of the trap cyclotron motion (37, 38).

3. FACILITY OVERVIEW: PENNING-TRAP MASS SPECTROMETERS

In 1976, Gärtner & Klempt (39) performed the first direct mass measurement using a Penning trap, first introduced by Dehmelt (40). Their proton-to-electron mass ratio determination was, however, performed at a lower precision than that of previous indirect measurements, primarily due to large space charge effects in the trap. Four years later, in 1980, Gräff et al. (22) measured

Table 1 Penning-trap mass spectrometers at radioactive ion beam facilities^a

Name	Year	Location	Facility	Reaction(s)
ISOLTRAP	1987–present	ISOLDE, CERN	ISOL	Spallation, fission
CPT	1998–2009	ATLAS, ANL	In-flight	Transfer, fusion–evaporation
CPT	2009–present	CARIBU, ANL	ISOL	²⁵² Cf fission
SHIPTRAP	2004–present	SHIP, GSI	In-flight	Fusion–evaporation
JYFLTRAP	2004–present	JYFL, Jyväskylä	IGISOL	Various
LEBIT	2005–present	NSCL, MSU	In-flight	Fragmentation
TITAN	2007–present	ISAC, TRIUMF	ISOL	Spallation, fission
TRIGATRAP	2017–present	TRIGA, Mainz	Reactor	Fission

^aThe year of operation starts with the first mass measurement of a radioactive ion. Abbreviations: IGISOL, ion guide–based isotope separation online; ISOL, isotope separation online.

this important mass ratio at a greater precision by using, for the first time, the ToF-ICR technique (see Section 2.2.1). This technique, now used routinely in every Penning-trap system at online facilities (see Section 3.1), was chosen over the previous method (39) due to its insensitivity to space charge effects, trap misalignment, and imperfections of the trap surface (22). Simultaneously, nondestructive techniques continuously improved, enabling substantial gains in precision for the determination of the proton-to-electron mass ratio (41), the proton-to-antiproton mass ratio (42), and the mass ratio of stable molecules (37). In the following subsections, we provide an overview of the various Penning-trap facilities dedicated to precision measurements of unstable (Section 3.1) and stable (Section 3.2) isotopes.

3.1. Penning-Trap Mass Measurements of Unstable Isotopes

Since the first measurement of cyclotron frequencies of radioactive rubidium (Rb) and strontium (Sr) ions at the Isotope Mass Separator On-Line facility (ISOLDE) at CERN in 1987 (43), ion trapping systems dedicated to perform high-precision mass measurements of unstable isotopes have flourished at several RIB facilities worldwide (Table 1). While these various experiments have overlapping capabilities, each of them benefits from distinctive features in terms of either what the RIB facility can deliver or the traps it includes. This makes all the facilities listed in Table 1 truly complementary.

3.1.1. Penning-trap systems coupled to radioactive ion beam facilities. The coupling of ion trap systems to RIB facilities opened up a completely new avenue for mass measurements in nuclear physics. By now, essentially all facilities that provide access to radioactive isotopes, whether generated by accelerators or from reactors, have some experimental system(s) using ion traps. Accelerator-based production systems, commonly referred to as online, are categorized into two groups: isotope separation online (ISOL)-type or in-flight RIB facilities (44).

ISOL production facilities typically employ proton beams as the primary driver and have that beam impinging on thick targets. Depending on the primary beam energy (ranging from 100 MeV to 1.4 GeV) and the target material, spallation, fragmentation, or fission reactions are induced. The newly synthesized isotopes resulting from these reactions are essentially neutral and at rest. Then the isotopes are ionized (44), and a beam of keV-range singly charged ions is formed, mass-separated, and delivered to experimental stations. A variation of the ISOL system is the so-called

ion guide–based ISOL (IGISOL) system, in which a tens-of-MeV-range primary beam impinges on a thin target, allowing the radioactive isotopes produced to recoil out of the target. These ions are then stopped in a gas and guided as a beam to a mass separator before being delivered to experimental stations. Other examples of facilities that use a buffer gas to collect and thermalize radioactive nuclei includes the CARIBU facility (45) and the nuclear reactor–based TRIGA-SPEC facility (11).

For the in-flight method, a 100–1,000 MeV/u heavy-ion beam impinges on a thin target. Fragmentation and fission reactions (depending on the primary beam and target material) take place. Due to the high energy of the primary beam, the synthesized isotopes continue to move forward as ions, and can be guided through a combination of electric and magnetic fields to achieve separation and/or identification of the products. In-flight separator systems, called fragment separators, are currently employed at the GSI Fragment Separator (FRS) (46), at RIKEN (47), and at Michigan State University’s National Superconducting Cyclotron Laboratory (NSCL) (48). Future systems are currently being designed or built for the Facility for Antiproton and Ion Research (FAIR) (49) and the Facility for Rare Isotope Beams (FRIB) (50). In-flight systems are also employed for fusion–evaporation systems such as SHIP at GSI (51) and ATLAS at Argonne National Laboratory (ANL) (52) and for transfer–reaction systems such as RESOLUT at Florida State University (FSU) (53) and TwinSol at the University of Notre Dame (54), where the primary beam energies are around 1–10 MeV/u.

3.1.2. Penning traps coupled to isotope separation online–type beam facilities. The first ion trap system to be coupled to a RIB facility was ISOLTRAP (55). The low-energy nature of the ISOL beam made this initial coupling relatively simple. Nevertheless, a Penning trap can capture only ions with energies of around 10–100 eV. Thus, in the initial stages of ISOLTRAP, the keV-range ISOL beam was first implanted into a foil in front of the Penning trap. The foil was rotated 180° and heated to release ions. The method was limited to surface-ionizable species but achieved remarkable results (56). In order to capture other species such as noble-gas elements into the Penning trap, an additional trap was employed. The extra trap, initially a hyperbolic trap (57) and later a more efficient linear Paul trap (58), could be floated on a comparable electrostatic potential as the incoming ion beam, enabling significant retardation to be achieved. The emerging bunched ion beam could be energetically matched for injection into the subsequent Penning trap. This method is currently used at all RIB facilities, both ISOL and in flight, as part of beam preparation prior to Penning-trap injection.

The ISOLTRAP system has evolved significantly (59) since its conception in the mid-1980s (55) and is currently composed of four traps in series (60): (a) a gas-filled linear Paul trap (58), (b) an electrostatic multireflector system [multireflection time-of-flight (MR-ToF)] mass separator (61), (c) a cylindrical preparation Penning trap (13, 62), and (d) a precision hyperbolic Penning trap used for mass determinations (13, 63). The ISOLTRAP system enables measurements of isotopes produced at very low intensities and is able to achieve a high level of suppression of coproduced contaminant isotopes. This is particularly important for neutron-rich isotopes. The Penning-trap system at ISOLTRAP can carry out mass measurements using the ToF-ICR and PI-ICR methods, and has performed experiments on isotopes as short lived as 65 ms (64) and covered isotopes ranging from ^{17}Ne to ^{234}Ra (59). The ISOLTRAP facility is very flexible and has been used on a wide variety of online-produced species. One of the unique features of ISOLTRAP is its coupling to a carbon-cluster ion source (65). Since the mass measurement relies on reference ions, it is important to have reference ions with known mass values available. Carbon atoms are used for the definition of the atomic mass unit and are therefore ideally suited to this purpose. Carbon clusters are molecules consisting of two or more carbon atoms, and hence represent a grid

of molecular reference ions at 12-mass unit separation. The powerful concept of carbon clusters as reference ions is now well established and has been applied at other online facilities (66–68).

The TITAN (TRIUMF's Ion Trap for Atomic and Nuclear Science) system is coupled to the Isotope Separator and Accelerator (ISAC) facility at TRIUMF (15, 69). The ISAC system (70, 71) is an ISOL-type RIB facility comparable to ISOLDE. TITAN originally operated in 2007 as a two-trap system combining a linear Paul trap [also referred to as an rf quadrupole (RFQ) ion cooler and buncher] (72) and a Penning trap (73). The system was used for very rapid mass measurements on isotopes with very short half-lives down to 9 ms (74). In the past decade, the TITAN system (75) has evolved to provide five trap systems in series; now following the RFQ trap is an MR-ToF system (76), a charge breeder electron beam ion trap (EBIT) (77), an electron-plasma cooler Penning trap (78), and a mass measurement Penning trap (73). The TITAN system is unique among online systems in that it provides charge breeding capabilities, allowing measurements on either singly or highly charged ions. The primary reason for highly charged ion measurements stems from the increased precision. Equation 2 introduces the relation of the mass-to-charge ratio to the cyclotron frequency. The increase in the charge state q leads to an increase of the absolute cyclotron frequency, which in turn enables one to achieve a higher relative precision. However, the charge breeding process introduces a number of effects that influence the reachable precision (79). First, while the charge breeding process leads to a charge state distribution, only one charge state can be transported into the Penning trap, leading to an effective efficiency loss. Second, the charge breeding process takes time, and depending on the radioactive isotope's half-life, some ions may decay prior to their injection into the Penning trap.

Nevertheless, charge breeding is very effective in performing high-precision measurements, as demonstrated with the short-lived isotope ^{74}Rb (80) and neutron-rich Sr and Rb isotopes (81). Moreover, the higher charge states allow for higher resolution in measurements of isomers (79, 82). In specific cases, charge breeding is used to generate unique configurations for the isotopes under investigation, as demonstrated by the use of so-called threshold charge breeding (83).

3.1.3. Penning traps coupled to in-flight systems. A drawback of the ISOL technique is its chemistry-dependent nature, where certain elements, such as the refractory ones, have very low diffusion rates from the target. In-flight production methods, by contrast, are more universal in that the recoiling radioactive species comes out of the thin target in the form of an ion beam. Such methods, however, produce a fast RIB (>1 MeV/u) with a large momentum spread that does not match the low energy and emittance requirements of Penning-trap systems. Various attempts to address this problem have been made.

The first system to be attached to an in-flight facility was the Canadian Penning Trap (CPT), after its move to ANL's ATLAS facility following the decommissioning of the Tandem Accelerator Superconducting Cyclotron (TASCC) at Chalk River in 1997 (84). The CPT at ATLAS included the devices that are now found in all Penning-trap mass spectrometers at in-flight facilities. First, the primary beam is separated from the forward recoils, and a first-order separation of some unwanted reaction products is performed. Second, the energy of the fast ions is reduced by use of a solid degrader prior to injection into a large-volume gas cell, where the ions thermalize via collisions with a helium buffer gas. Third, a combination of static and dynamic electrical fields is used to drag the ions in the gas volume up to an orifice where the large gas flow carries the ions into the adjacent evacuated chamber. Fourth, at the extraction side of the gas cell, a series of RFQs guides the ions through a series of differentially pumped sections before reaching ultrahigh vacuum. Past that stage, Penning-trap mass spectrometers at in-flight facilities comprise all the required components of their counterparts located at ISOL facilities: an RFQ trap to cool and bunch the beam and a precision Penning trap where the measurement is performed. Similar to

ISOLTRAP, the CPT at ATLAS also included a gas-filled Penning trap for removal of isobaric contamination. The CPT at ATLAS performed extensive measurements of the rapid proton capture process (rp-process) and of superallowed $0^+ \rightarrow 0^+$ pure Fermi β transitions to test the unitarity of the Cabibbo–Kobayashi–Maskawa (CKM) matrix.

The second Penning-trap mass spectrometer at an in-flight facility to become operational (85) was SHIPTRAP (86) at the SHIP velocity filter of GSI. SHIPTRAP was also the first facility to have both its purification trap and measurement trap housed in the same superconducting magnet. SHIPTRAP has found its niche in the mass measurement of heavy and superheavy nuclei.

The third and last Penning-trap mass spectrometer at an in-flight facility to become operational (87) is LEBIT (88) at Michigan State University’s NSCL. LEBIT is the only Penning-trap mass spectrometer to be located at a projectile fragmentation facility. LEBIT typically takes a cocktail beam of isotonic fragments from the A1900 fragment separator that have been thermalized in a large-volume gas cell. Another distinctive feature of LEBIT is its use of a 9.4-T magnetic field for its Penning trap, the largest of any RIB trapping facility, which provides enhanced resolving power.

3.1.4. Other Penning traps coupled to gas stopper-based beam systems. Although the Penning-trap mass spectrometers discussed in this subsection are not coupled to an in-flight system, they all make use of RIBs coming from the thermalization of ions in a high-pressure gas cell. The first system to be attached to a high-pressure gas cell was the CPT, in its original location at the now-defunct TASCC at Chalk River (1995–1997). There, the CPT was planned for use as a system combining an aerosol-loaded helium jet with a pulsed laser to collect and reionize the radioactive nuclei produced after the impact of the heavy-ion beam from TASCC on a series of thin targets (89). Such systems resemble ISOL beam production but are universal, since the reaction products come out of the thin targets.

The IGISOL technique, developed in the mid-1980s in Jyväskylä, Finland, was also a compromise between the high power and production rates of the ISOL technique and the universality of in-flight production. An IGISOL system typically comprises a thin target followed by a small, high-pressure helium gas volume. A beam of light ions from a cyclotron then impinges on the target, producing radioactive nuclei that recoil out of the target into the gas volume, where some of them thermalize. Because a small gas volume is used, only the gas flow brings the ions out of the stopping cell and into the differentially pumped region where the ions are guided using a sextupole ion guide. The JYFLTRAP system (12)—which, like SHIPTRAP, has both its purification and measurement traps housed in the same superconducting magnet—has been measuring unstable nuclei produced by the IGISOL technique since 2004 (90). The universality of the IGISOL technique coupled to a beam delivery that is simpler than that in fragmentation facilities has allowed JYFLTRAP to cover large regions of the chart of nuclides.

The TRIGATRAP Penning trap (11), located at the TRIGA reactor at the University of Mainz, is the only Penning-trap mass spectrometer connected to a research nuclear reactor. Radioactive nuclei are produced via thermal neutron-induced fission on actinide targets. High yields of these products are expected from the large neutron flux and the large thermal neutron fission cross section. The target system shares some similarities with the CPT at TASCC in that the fission products recoiling from the thin target thermalize in a carrier gas loaded with aerosols and are then transported, using a capillary, up to an ion source. After the ion source, the ion beam is transported to an RFQ cooler and buncher and the double Penning-trap system (housed in the same magnet). Although TRIGATRAP has not performed online measurements using fission products from the reactors, it has carried out several measurements of laser-ablated stable (91) and long-lived nuclei (92).

In 2009, the CPT moved to the CARIBU facility at ANL (45). At CARIBU, the products of the spontaneous fission of ^{252}Cf stop in a large-volume gas cell (93), which has the same working principle as the one used at ATLAS (described in the previous section). After an extraction ion guide, a large fraction of the molecular and radioactive contamination produced in the gas cell is separated using a high-resolution (around 12,000) separator before being injected into an RFQ cooler and buncher. The ion bunches are further purified through the removal of isobaric contaminations by use of a multireflection mass spectrometer (94). Finally, the purified bunches are sent to a cryogenic RFQ for further cooling and ion rebunching prior to insertion in the Penning trap (95).

3.2. Penning-Trap Mass Measurements of Stable Isotopes

Applications of precision mass data to, for example, neutrino physics or tests of fundamental interactions require relative mass uncertainties of 10^{-10} and below. In almost all cases, the nuclides of interest are either very long lived or stable. Therefore, coupling to an online facility is not necessary, and samples for ion production can be prepared offline. Dedicated Penning-trap installations, discussed below, have been developed in order to perform such measurements. With the exception of SMILETRAP in Stockholm, which is no longer in operation, all of these setups use a nondestructive ion detection technique (described in Section 2.2.3).

Concerning mass precision in absolute mass measurements, the leading installation is the Penning-trap mass spectrometer that has been located at FSU since 2003 (previously, it was located at MIT). Mass ratio measurements with an uncertainty of only 7×10^{-12} were demonstrated at MIT through the so-called double-pan technique (5), and mass uncertainties of approximately 10^{-11} were demonstrated at FSU (3). A unique feature of this apparatus is the use of a superconducting quantum interference device (SQUID) system for detection of the image current induced in a superconducting tuned circuit.

The University of Washington's Penning-trap mass spectrometer, which in 2008 moved to the Max Planck Institute for Nuclear Physics (MPIK) in Heidelberg (18), has demonstrated a mass precision similar to that of the spectrometer at FSU (41). The superconducting magnet holds the record for the most stable magnetic field with a relative variation of less than 10^{-11} h^{-1} , which enables long observation and measurement times of several hours. SMILETRAP used the ToF ion cyclotron detection technique in combination with highly charged ions, which allowed for mass uncertainties in the 10^{-10} regime even for heavy species above $A = 200$ (96). Unfortunately, SMILETRAP was shut down in 2010. A new approach called PENTATRAP using highly charged ions from an EBIT in a multi-Penning-trap system for high-precision mass measurements on heavy species was recently launched at MPIK (19). For mass measurements on light systems such as the proton, the former Mainz g -factor experiment on highly charged ions was rebuilt and put into operation (97).

Many modern experiments in the field of fundamental physics make high demands on high-precision Penning-trap mass spectrometry with regard to achievable precision in the mass determination of a variety of long-lived and stable nuclides. Several next-generation experiments on the determination of the neutrino mass, such as the ECHo project (98), exemplify the complexity of the tasks that Penning-trap mass spectrometry is facing. In order to determine the neutrino mass on a sub-eV level, it is necessary to measure the Q values of certain β transitions with an unprecedentedly low (and so far unachievable) uncertainty below 1 eV.

The inability of high-precision mass spectrometers to provide such high precision demands the creation of next-generation Penning-trap facilities capable of measuring the masses of long-lived nuclides with a relative accuracy substantially better than 10^{-11} . PENTATRAP is just such a

next-generation Penning-trap mass spectrometer, and is currently being set up at MPIK (19, 20). The design of the facility is dictated by the intended precision. It is mandatory that the nuclides under investigation be highly ionized, which requires two EBIT ion sources: (a) Dresden-EBIT3 (see <http://www.dreebit.com>; status on September 28, 2017) and (b) Heidelberg-EBIT (99). Dresden-EBIT3 is a commercial compact EBIT that allows production of, for instance, heavy nuclides such as rhenium up to a charge state of approximately 50^+ . It serves as a test ion source for optimizing the performance of the mass spectrometer. The first mass measurements with PENTATRAP will be carried out with the Dresden-EBIT3. The Heidelberg-EBIT is a powerful superconducting ion source that, after a planned upgrade, will be capable of delivering to the PENTATRAP experiment fully ionized long-lived nuclides up to lead. The EBIT ion sources are interfaced with the Penning-trap mass spectrometer with a several-meter-long ion transport beam line, which contains a series of electrostatic Einzel and quadrupole lenses, pulsed drift tubes, a 90° bending magnet, and ion beam diagnostic stations for monitoring the quality of the ion beam at key positions in the beam line. The electrostatic lenses enable efficient transport of the ions toward the mass spectrometer. The pulsed drift tubes are used to reduce the kinetic energy of the ions from a few kilovolts per unit charge down to a few volts per unit charge to ensure, together with the lens system, an efficient injection of the ions into the mass spectrometer, and to enable the ions to be captured in the traps.

The heart of the facility is a one-of-a-kind cryogenic Penning-trap mass spectrometer. It is located in a dedicated laboratory with a stabilized environment and comprises a highly stable, actively shielded 7-T superconducting magnet with a vertical cold bore that houses an array of five cylindrical Penning traps. The feasibility of reaching a sub-eV level of mass determination rests on several pillars: (a) a multitrap configuration, which will enable, for the first time, simultaneous measurement of two nuclides and continuous monitoring of the magnetic field fluctuations during the entire measurement process, (b) an ultrastable source of trap electrical potentials, which has been developed by the MPIK electronic workshop in collaboration with PTB Braunschweig, (c) a shield protecting the trap from stray electric and magnetic fields and mechanical vibrations, (d) stabilization of the temperature in the lab at the level of 0.1 K per day, and (e) use of the novel PnA mass measurement technique introduced by Sturm et al. (38), which is based on a nondestructive phase-sensitive image-current detection technique and provides single-ion sensitivity.

All of the key components of PENTATRAP have been successfully tested and are presently in different phases of optimization. The entire facility has been assembled, and the complete cycle—including production of various highly charged ions (argon, xenon, rhenium) with the Dresden-EBIT3 ion source, ion transport to the mass spectrometer, capture of a single highly charged ion in the central trap, and detection of the ion's presence in the trap through measurement of its axial frequency—has been successfully tested. Furthermore, a sophisticated system to minimize environmental effects on the mass spectrometer has been installed and tested. Extensive efforts to improve the mass spectrometer's performance are under way.

The Central Michigan University High-Precision Penning Trap (CHIP-TRAP) (21) will consist of a pair of hyperbolic geometry Penning traps and a cylindrical capture trap in a 12-T magnetic field. A pair of single ions will be stored in the measurement traps for simultaneous cyclotron frequency comparisons, which will greatly reduce statistical uncertainty due to magnetic field fluctuations. CHIP-TRAP will utilize techniques employed by online Penning-trap facilities to transport ions from external ion sources, including a laser ablation ion source, to the Penning traps. The ion transport will allow ions of a given mass-to-charge ratio to be selected via their ToF by use of a fast electrostatic gate. Ions will be captured in the capture trap, where isobaric contamination can be identified and removed using FT-ICR techniques. The ions of interest will then be transported to the precision measurement traps.

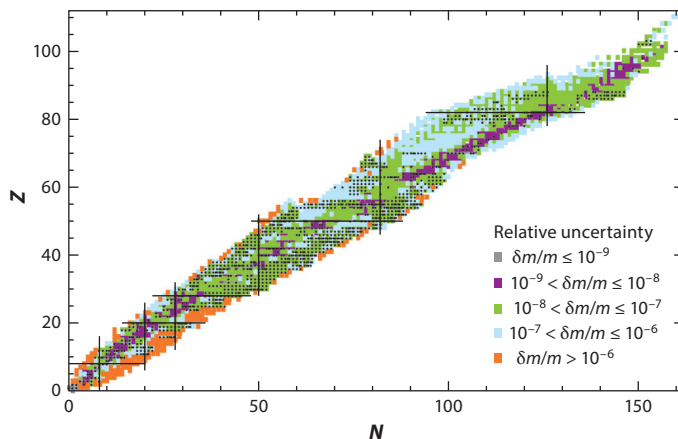


Figure 5

Relative uncertainty on the experimental atomic masses from the 2016 atomic mass evaluation (AME2016) (100). Known nuclear shells are indicated by solid lines. Isotopes measured using a Penning trap are indicated by black dots.

4. NUCLEAR PHYSICS APPLICATIONS

High-precision nuclear mass data have broad applications in nuclear physics research, including nuclear structure, nuclear astrophysics, and fundamental studies. Currently, more than 3,300 different nuclides across the nuclear chart are known, most of which are accessible by Penning-trap mass spectrometry. **Figure 5** depicts the current status of the relative mass uncertainty (100) for the approximately 2,500 known atomic masses (101). Precision nuclear mass data provide information about, for example, the path of the proton and neutron drip lines (i.e., where protons and neutrons become unbound in the nucleus), the possible location of the island of stability in the superheavy mass region, shell effects and magic numbers, and the strength of proton and neutron interactions.

4.1. Mass Measurements for Nuclear Structure Studies

Atomic masses are an important probe of changes in the structure of the nucleus because the atomic mass is directly related to the nuclear binding energy, which is the sum of the interactions holding the nucleons together. Historically, improvements in atomic mass measurement precision played an important role in the discovery of the so-called magic numbers, which led to the formulation of the nuclear shell model (102). Furthermore, the first mass measurements on neutron-rich sodium isotopes using a classical mass spectrograph at CERN provided the first experimental evidence of the vanishing of $N = 20$ magicity (103). Evidently, the development of a more accurate and precise technique, Penning-trap mass spectrometry, and its application to unstable nuclei led not only to the discovery of more shell-structure changes but also to other key scientific advances in the broader field of nuclear structure. In the following subsections, we discuss progress during the past decade in our understanding of shell evolution, deformation, halo nuclei, and superheavy nuclei stemming from high-precision Penning-trap mass measurements.

4.1.1. Separation energies. Whereas evidence for the nuclear shell structure from atomic masses originally came from the underestimation of the liquid drop model binding energies in comparison

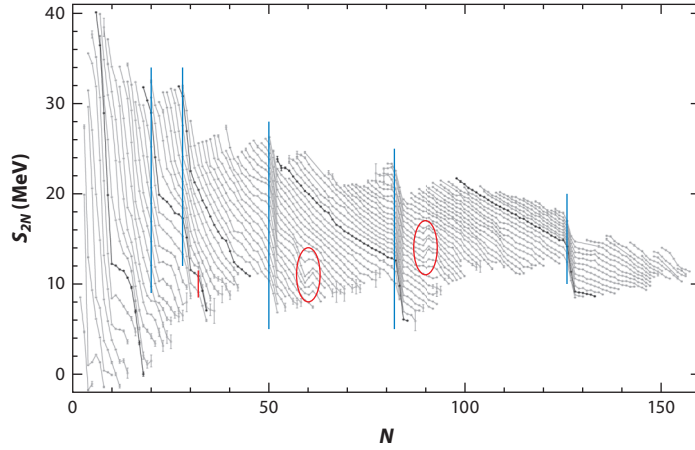


Figure 6

Two-neutron separation energies S_{2N} from the experimental masses of the 2016 atomic mass evaluation (AME2016) (100) from $Z = 1$ to 100. Magic numbers $N = 2, 8, 20, 28, 50, 82, 126$ are indicated by blue vertical lines over the range where they are observed. Isotopes with $Z = 8, 20, 28, 50$, and 82 are connected by thick black lines to guide the eye. The electroweak magic number $N = 32$ is indicated by a red vertical line. Regions of rapid shape transitions are indicated by red ovals.

to experimental values for magic number nuclei (2), such shell structure can actually be observed model independently by use of mass differences. The quantity commonly used to portray the effect of the shell structure on atomic masses is the two-neutron separation energy, $S_{2N} = m(N-2, Z) + 2m_n - m(N, Z)$, which corresponds to the energy required to detach two neutrons from the nucleus. This quantity is usually preferred over the one-neutron separation energy because it removes the staggering effect in energy caused by the two-neutron pairing. **Figure 6** shows the S_{2N} values of all known masses from the 2016 atomic mass evaluation (AME2016) (100). Notable features include the general decrease in S_{2N} with neutron number, larger drops around $N = Z$, and the increase in S_{2N} with Z , all of which can be explained by the asymmetry term of the liquid drop model. The magic numbers $N = 2, 8, 20, 28, 50, 82$, and 126 can be clearly observed as a large drop in S_{2N} at these values. This large drop can be explained by the fact that it would require less energy to remove the first two neutrons that are filling the energy level above the shell gap. The $N = 2$ and 8 magic numbers are more difficult to see in **Figure 6** due to the competing effect of the larger asymmetry and Wigner energy terms for light nuclei. Another notable feature of **Figure 6**, which we discuss in the next section, is the change in nuclear shape, indicated by an increase in S_{2N} .

4.1.2. Change in magicity. Shell closures in calcium isotopes have attracted greater attention since the prediction of new magic numbers at $N = 32$ and 34 approximately a decade ago (104). A series of mass measurements at TITAN (105, 106) and ISOLTRAP (107, 108), which benefit from their high yields of neutron-rich calcium (Ca) and potassium (K) beams, have greatly improved our understanding of these shell closures. First, mass measurements of neutron-rich K isotopes up to ^{51}K at TITAN have shown a resurgence of the $N = 28$ shell gap in K (105). The subsequent direct mass measurement in this region, also performed at TITAN, revealed a 1.7-MeV deviation in the mass excess of ^{52}Ca , which led to better agreement with theoretical predictions (106). Of particular interest are the ISOLTRAP mass measurements of $^{53,54}\text{Ca}$, performed with the MR-ToF mass spectrometer, which unambiguously confirmed the $N = 32$ shell closure (107). Finally,

the mass measurements of neutron-rich K isotopes at ISOLTRAP (108) have revealed both the doubly magic nature of ^{54}Ca and the retention of the $N = 32$ shell closure for ^{53}K (Figure 6).

4.1.3. Deformation. Deformed nuclear ground states are known to have a different single-particle energy level structure from that of their spherical counterparts; they also present extra collective degrees of freedom. Thus, the deformation of the nucleus affects its binding energy. For this reason, modern nuclear mass models typically include terms to account for nuclear deformation.

Just as for shell closures, changes in the nuclear shape can be regarded as deviations from the regular decrease in S_{2N} values expected from the liquid drop model. The transition from a spherical to a deformed ground state results in an increase in S_{2N} (Figure 6).

Several campaigns at JYFLTRAP and ISOLTRAP have shed light on some of these regions of deformation. Particularly important are a systematic series of measurements of neutron-rich isotopic chains from $Z = 38$ to 46 at JYFLTRAP (109–112), which have revealed a pronounced increase in S_{2N} values due to a rapid shape transition around $N = 60$ (Figure 6).

4.1.4. Nuclear halos. One of the challenges of modern nuclear theories involves the correct prediction of multiple properties of nuclides along larger regions of the chart of nuclides. Nuclei forming a neutron halo structure at their ground state provide very stringent tests of nuclear theories (113). Neutron halos comprise a core that includes most of the nucleonic matter except for one to four decoupled, loosely bound neutrons that form the halo structure (114). While knowledge of the size of the core, its shape, and its motion relative to the center of mass can be obtained from a determination of the nuclear charge radius, the extent of the diffuse halo region, due to the quantum-mechanical leakage of the valence neutron wave function, depends exponentially on the valence neutron separation energy. Precise and accurate atomic masses are important not only for the determination of neutron separation energies but also, indirectly, for the determination of the charge radius. Isotopic shift measurement is currently the only model-independent way to determine the charge radius of radioactive nuclei (115). In order to extract a charge radius from that type of measurement, one requires a precise determination of the so-called mass shift, which depends sensitively on atomic masses. Therefore, a series of high-precision mass measurements on the halo nuclei ^6He (116), ^8He (116, 117), ^{11}Li (74), and ^{11}Be (118) were undertaken at TITAN, which benefited from the high ISAC rates for these nuclei. The very high repetition rates that TITAN can handle (119) in comparison to other Penning-trap systems was another crucial factor that enabled mass measurement of the 8.8-ms half-life of ^{11}Li (74). Because of the confining effect of the Coulomb barrier, proton halos are less pervasive than their neutron counterparts. The atomic mass of one of the main two-proton halo candidates under study, ^{17}Ne , has been measured by ISOLTRAP (120).

4.1.5. Superheavy nuclei. The exact location of the next nuclear shells beyond $Z = 82$ and $N = 126$ is one of the critical questions in nuclear structure remaining to be addressed. Significant experimental efforts to produce new isotopes and even elements leading to the purported island of stability are under way. Precise and accurate atomic masses of the lighter end products of the α decay chains of these superheavy nuclei are particularly important because they would provide the necessary anchor points from which the atomic masses of superheavy nuclei could be determined. The SHIPTRAP Penning-trap system (9), located at the SHIP facility at GSI, has found its niche in the mass measurement of these very heavy systems because of the SHIP facility's unique capabilities (10, 121, 122).

4.2. Mass Measurements for Nuclear Astrophysics Studies

Nuclear astrophysics is concerned with the understanding of the creation and propagation of the chemical elements and their corresponding abundances in the Universe, as well as with the influence of nuclear physics on the evolution of stars and stellar objects (123). The masses of the participating isotopes in all of these processes play crucial roles. The atomic mass influences the nuclear reaction rates and is a direct parameter in network calculations (124, 125). Such calculations allow one to study and delineate process paths, in particular the rp-process and the rapid neutron capture process (r-process), which are considered to involve very proton-rich or neutron-rich isotopes, respectively.

4.2.1. Mass measurements for the r-process. The synthesis of approximately half of the elements heavier than iron, reaching up to uranium, is believed to be produced under extreme conditions in what is known as the r-process (126, 127). The astronomical site(s) of this process has been a contentious topic for many years (128, 129), but the recent simultaneous observation of a gravitational wave (130) and a kilonova from a neutron star merger (131) has now confirmed such systems as being one of the production sites of the r-process (132). Thus, it is now more imperative than ever to have reliable nuclear physics inputs for the abundance calculations of the r-process.

Several detailed sensitivity studies (125, 133) have been performed to identify which experimental quantity has the greatest leverage on the abundance pattern, as well as to prioritize which nuclei should be studied first. As a result of these studies, atomic masses, which enter in the calculation of nearly all quantities involved in the process (including neutron separation energies, β decay rates, and neutron capture rates), were unsurprisingly found to be the most critical experimental quantity (125). At the same time, the important regions of the chart of nuclides to investigate were found to be consistently south of the $N = 82$ and $N = 126$ closed shells, as well as in the so-called rare-earth region (125).

Because the r-process proceeds essentially in uncharted regions of the nuclear chart, one has to rely on mass models for the network calculations. These mass models use known atomic masses closer to stability as anchor points. Thus, it is crucial to have both precise and accurate masses in the region. Once again, because Penning-trap mass spectrometry meets both of these requirements, it has proven to be, when production rates allow, the method of choice.

Mass measurements for the r-process represent a combined effort from multiple groups located in laboratories with complementary capabilities. The ISOLTRAP and TITAN experiments, located at ISOL facilities, benefit from the highest rates of the cleanest and most exotic isotopes of certain elements. This allowed both experiments to reach unprecedented neutron richness in Rb and Sr (81, 134–136), as well as cadmium (Cd) isotopes (137). Many elements, however, cannot be accessed by the ISOL method. In these cases, the experiments need to be performed at a facility that produces the RIB more “universally.” The CPT and JYFLTRAP experiments, located at the CARIBU and IGISOL facilities, respectively, employ a RIB produced via the fission product of heavy actinides, collected in a gas volume, and subsequently formed as a low-energy RIB. The neutron-rich location of the two fission humps near the $N = 82$ shell and the rare-earth region has allowed both experiments to perform mass measurements on vast regions important for the r-process (95, 138, 139). Furthermore, the slight difference in the distribution in fission yield between the spontaneous fission of ^{252}Cf at CARIBU and the proton-induced fission $^{\text{nat}}\text{U}$ at IGISOL (and ISOL in general) offers complementary reach (139).

The greatest challenge facing current facilities in performing mass measurements for the r-process is the simultaneous minute production of the nuclei of interest and the large production

of isobaric contamination, which is for the most part molecular. Such contamination must be removed through the usual means discussed above, including dipole excitation in the preparation Penning trap (at JYFLTRAP and ISOLTRAP), dipole excitation in the measurement trap (at all facilities), Ramsey cleaning (at JYFLTRAP), and the more recent use of MR-ToF mass spectrometers (at ISOLTRAP, TITAN, and the CPT). The phase-image technique, which enables greater resolution and the separation of the remaining contaminants from the ion of interest, is now routinely used at the CPT and ISOLTRAP to measure radioactive nuclei of interest for the r-process.

4.2.2. Mass measurements for the rp-process. On the proton-rich side, high-precision mass measurements have also played an important role in formulating a better understanding of the rp-capture process (124). In contrast to the r-process, however, the astronomical location of the rp-process is well known. The process occurs at the surface of a neutron star that is accreting material from a large companion star. As more material is accreted, the density and temperature increase, resulting in a thermonuclear runaway. The large increase in temperature also results in a sharp increase in X-ray luminosity, generating a type I X-ray burst (140).

At the surface of the neutron star, nuclei undergo rapid proton capture, combined with β decays forming a path along the neutron-deficient part of the chart of nuclides (141, 142). Although the rp-process synthesizes proton-rich nuclei, it does not play an important role in the production of the elemental abundances observed. This is because any material that could be released from the burst falls back onto the surface of the neutron star due to its large gravitational field.

Many Penning-trap experiments have improved our understanding of the rp-process and the accompanying X-ray light curve. The CPT, when it was using a RIB produced in flight at ATLAS, measured several critical nuclei not only for the rp-process (143) but also for the vp-process (144). The LEBIT experiment at the NSCL also measured several nuclei in the regions near $N = Z = 33$ (145) and $N = Z = 34$ (146). ISOLTRAP measured several masses important for the rp-process above $Z = 32$ (147). SHIPTRAP performed mass measurements near the endpoint of the rp-process (148).

Finally, JYFLTRAP measured several nuclei of interest for the rp-process, including proton-rich molybdenum, technetium (149), and nuclides in the vicinity of the waiting point ^{56}Ni (150); it also discovered SnSbTe cycle quenching in the rp-process (151) and carried out a combined campaign with SHIPTRAP (152). More recently, ^{31}Cl (153), ^{52}Co (154), and ^{25}Al and ^{30}P for classical nova studies (155) have been measured.

5. MASS MEASUREMENTS FOR FUNDAMENTAL PHYSICS TESTS

5.1. Mass Measurements for Neutrino Physics Studies

Among the fundamental particles, the neutrino is considered one of the most mysterious. Predicted by theory (156) and discovered in 1956 (157), the neutrino had long been thought to be massless, as the Standard Model of particle physics (SM) assumes. There are three different types of neutrinos—electron ν_e , muon ν_μ , and tau ν_τ —that in nuclear processes accompany electrons, muons, and tauons, respectively. A recent observation of neutrino oscillation (158) has revealed astounding facts about neutrinos. First, despite the prediction of the SM, neutrinos do have mass. Second, neutrinos observed in experiments are of three leptonic flavors—incoherent sums of three neutrino mass states with very small and similar masses. Third, the smallness of neutrino masses, compared with the masses of other SM fermions, is often attributed to the fact that neutrinos, lacking charge, can have two kinds of masses (Dirac and Majorana).

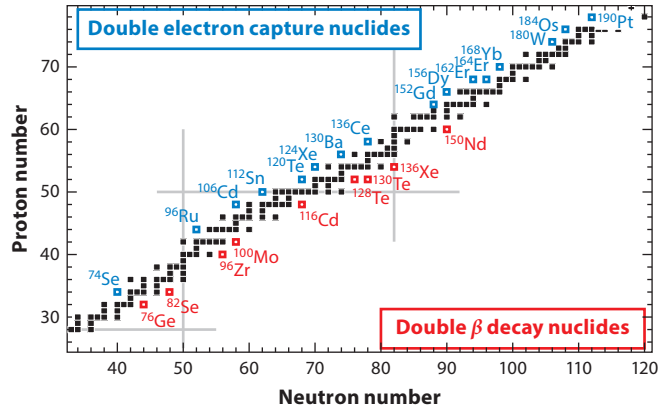


Figure 7

Nuclides that undergo double β decay processes and are of interest for the determination of neutrino type. Adapted with permission from Reference 115.

Despite rapid progress in the investigation of neutrino properties, the list of open issues is long. The following three are probably the best known to nonspecialists. First, the absolute neutrino mass value is not known. Second, as neutrinos lack charges or any other additively conserved quantum numbers that would distinguish them from their antiparticles, they can have both Majorana and Dirac masses. The other SM fermions are charged and thus are Dirac particles. Third, it is not certain that there exist only active neutrinos. Some extensions of the SM predict the existence of so-called sterile neutrinos—neutrinos that do not undergo weak interaction but can mix with active neutrino mass states with certain mixing angles (159, 160).

Answers to these open questions could be obtained from the investigation of nuclear β processes in certain long-lived nuclides: β^- decay (161), EC (161), neutrinoless double β^- decay ($0\nu 2\beta^-$ decay) (162) and neutrinoless double electron capture ($0\nu 2\text{EC}$) (163). This investigation demands independent and direct determination of the Q values of the β processes involved with a very low uncertainty. High-precision Penning-trap mass spectrometry is the right (and, moreover, the only) tool that is capable of providing the Q values with the needed uncertainty via measurements of the mass differences of the parent and daughter nuclides of the β processes under investigation.

5.1.1. Types of neutrinos. Some virtually stable nuclides (Figure 7), which are situated in the nuclear chart on both sides of the valley of β stability, can undergo very exotic and extremely rare processes. They can emit two electrons or can capture two atomic orbital electrons; either there is emission of two neutrinos, or these processes can be neutrinoless. The two-neutrino mode can take place independently of the neutrino type and hence is of little use in the determination of the neutrino type. The process of interest here is the neutrinoless mode. A mere observation of this process would be an unambiguous proof that neutrinos and antineutrinos are identical particles. Furthermore, a measurement of the neutrino half-life would, in principle, allow a determination of the effective Majorana neutrino mass (162). Several large-scale experiments are devoted to the search for $0\nu 2\beta^-$ decay (164). In these experiments, one searches in the energy-sum spectrum of two emitted electrons for a peak at an energy corresponding to the Q value of the investigated double β^- decay (Figure 8). This search is hampered by a continuous spectrum originating from the much more probable two-neutrino mode. To localize in the energy spectrum the range of interest where this peak is supposed to appear, one needs to know the Q value of the process with an uncertainty of approximately 1 keV. Furthermore, for the determination of the effective

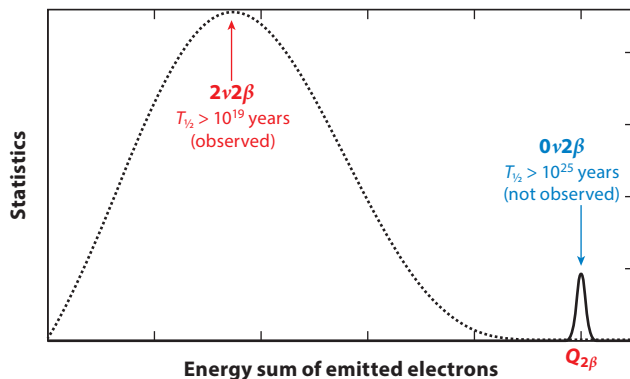


Figure 8

Energy-sum spectrum of two emitted electrons in double β^- decay. The neutrinoless mode reveals itself as a peak at an energy that corresponds to the Q value of the process. The continuous spectrum below the Q value originates from the much more probable two-neutrino mode.

Majorana neutrino mass from the measurement of the half-life of this process, it is desirable to know the Q value with a sub-keV uncertainty. Such uncertainties are easily achievable at all modern high-precision Penning-trap facilities, and the Q values of all the most prominent double β^- decay transitions have been already determined by various Penning traps with sufficiently low uncertainty (**Table 2**) (165–173). The situation with the search for $0\nu 2\text{EC}$ is more dramatic. It could be as probable as $0\nu 2\beta^-$ decay only if it is resonantly enhanced (163). In that case, $0\nu 2\text{EC}$ would offer some benefits with respect to $0\nu 2\beta^-$ decay (174):

- There are a variety of excited nuclear states with different low spin values and different parities in one nuclide to which the double EC transition can be resonantly enhanced, resulting in relatively short partial half-lives.
- There is a possibility of testing the existence of the right-handed lepton current by observing transitions to nuclear excited states with negative parity.
- There is no essential background from the two-neutrino mode in the subsequent monochromatic spectrum of the neutrinoless mode.

In order to assess whether a particular $0\nu 2\text{EC}$ transition is resonantly enhanced, one has to determine its Q value with a 100-eV uncertainty.

Table 2 Double β^- decay transitions of greatest interest in the search for $0\nu 2\beta^-$ decay and their Q values measured with high-precision Penning-trap mass spectrometry

Transition	Q value	Reference
$^{136}\text{Xe} \rightarrow ^{136}\text{Ba}$	2,457.83(37)	165
$^{76}\text{Ge} \rightarrow ^{76}\text{Se}$	2,039.006(50)	166
$^{130}\text{Te} \rightarrow ^{130}\text{Xe}$	2,527.518(13)	167
$^{100}\text{Mo} \rightarrow ^{100}\text{Ru}$	3,034.40(17)	168
$^{82}\text{Se} \rightarrow ^{82}\text{Kr}$	2,997.9(3)	169
$^{116}\text{Cd} \rightarrow ^{116}\text{Sn}$	2,813.50(13)	170
$^{48}\text{Ca} \rightarrow ^{48}\text{Ti}$	4,268.121(79)	171
$^{150}\text{Nd} \rightarrow ^{150}\text{Sm}$	3,371.38(20)	172
$^{96}\text{Zr} \rightarrow ^{96}\text{Mo}$	3,356.097(86)	173

An extensive experimental campaign has recently been undertaken in order to find a resonantly enhanced $0\nu 2\text{EC}$ transition. In this campaign, the Q values of 15 double EC transitions of interest have been determined at various high-precision Penning-trap facilities with sufficiently low uncertainty (174, 175). Two $0\nu 2\text{EC}$ transitions have been found to be at least partially resonantly enhanced: (a) $^{152}\text{Gd} \rightarrow ^{152}\text{Sm}$ (176) between the nuclear ground states and (b) $^{156}\text{Dy} \rightarrow ^{156}\text{Gd}$ (177) between the nuclear ground state of the parent nuclide and a nuclear excited state of the daughter nuclide with energy and spin of 1,988.5(2) keV and 0^+ , respectively. The expected half-lives of these transitions, normalized to the effective Majorana neutrino mass value of 1 eV and estimated on the basis of measured Q values and of the calculations of their nuclear matrix elements, exceed 10^{26} years eV^{-1} . Such half-lives are still out of the reach of modern experiments. Thus, although a search for $0\nu 2\text{EC}$ might be in some aspects advantageous over a search for $0\nu 2\beta^-$ decay, all efforts in the near future will be focused on the search for $0\nu 2\beta^-$ decay.

5.1.2. Neutrino mass. There are three established ways to determine the neutrino mass. First, current combined analyses of the standard cosmological model constrain the energy density in relativistic particle species, from which one can deduce a bound on the sum of the neutrino masses. Second, the measurement of the half-life of neutrinoless double β processes can enable determination of the effective Majorana neutrino mass. Third, investigation of β processes (β^- decay and EC) is the most convenient method to determine the mass of one of the neutrino flavor states: the electron neutrino. The last is the only model-independent way to determine the neutrino mass.

The most stringent limit on the electron neutrino mass, $2.0 \text{ eV}/c^2$ (95% CL), was obtained by the combined Troitsk neutrino mass experiment and Mainz neutrino mass experiment from the analysis of the β^- decay of tritium (178–180). At present, five experiments are under construction with the goal of pushing this limit well below $1 \text{ eV}/c^2$. They are based on the analysis of the endpoint region of either the β^- decay spectrum of tritium (181) or the atomic de-excitation spectrum of the EC in ^{163}Ho (182, 183). The Q values of these processes, measured directly and independently by high-precision Penning-trap mass spectrometry, will facilitate an assessment of the systematic uncertainty in the neutrino mass determination.

The most advanced experiment on the determination of the neutrino mass from the tritium β^- decay—the KATRIN project (181)—requires a measurement of the Q value of the tritium β^- decay with an uncertainty of, at most, a few tens of meV/c^2 . The FSU trap has recently made a big step toward this goal by determining the Q value of the tritium β^- decay with a 70-meV uncertainty by measuring the mass difference of tritium and ^3He (3). Another Penning-trap mass spectrometer, the THe trap (184), is being set up especially to provide the KATRIN experiment with a sufficiently precise Q value of the tritium β^- decay. Finally, Project 8 of the University of Washington aims to determine the neutrino mass by using cyclotron radiation emission spectroscopy (185).

A rapidly developing cryogenic microcalorimetry technique forms the basis for experiments on the determination of the neutrino mass from the analysis of the EC in ^{163}Ho . The contribution of high-precision Penning-trap mass spectrometry to these experiments is chronologically divided into two phases: a preparatory phase and a main phase. The preparatory phase is required in order to determine the scale of these experiments. Here, the Q value of the EC in ^{163}Ho was determined with SHIPTRAP with an uncertainty of approximately 30 eV (4) by use of the PI-ICR technique (23, 33). This has solved a long-standing problem concerning the substantial disagreement between the Q values obtained with different techniques and has confirmed the accuracy of the Q values obtained with cryogenic microcalorimetry. The main phase consists of measuring the Q value of the EC in ^{163}Ho with an uncertainty of approximately 1 eV, which will enable determination of the neutrino mass on a sub- eV/c^2 level. Realization of the main phase will become feasible with the

Penning-trap mass spectrometer PENTATRAP, which is being built at MPIK (19, 20). Another project under development, CHIP-TRAP, also aims to determine the Q value of the EC in ^{163}Ho with eV uncertainty (21).

5.2. Test of the Standard Model via Weak Interaction Studies

High-precision Penning-trap mass spectrometry plays an important role in fundamental studies, such as in testing the SM. The SM is one of the pillars of modern physics and combines our knowledge about all known elementary particles and three of the four known fundamental forces (electromagnetic, weak, and strong forces) that describe the interactions between their particles. Thus, verification of its validity is the focus of a variety of modern experiments. Even more interesting would be a discovery of the violation of the SM's validity in some physical processes, which would hint at New Physics.

One means of testing the SM is to use the CKM matrix, which relates the quark weak interaction eigenstates to the quark mass eigenstates. Nonunitarity of the CKM matrix would imply violation of the validity of the SM in the weak interaction.

The CKM matrix is a 3×3 matrix. Its unitarity implies the fulfillment of the following expression for its top-row elements V_{uj} :

$$\sum_j |V_{uj}|^2 = |V_{ud}|^2 + |V_{us}|^2 + |V_{ub}|^2 = 1. \quad 11.$$

With a contribution of approximately 95%, V_{ud} is the largest term in this sum; thus, the uncertainty in its determination defines the overall uncertainty of our knowledge of Equation 11. This leading element can be derived from the investigation of $0^+ \rightarrow 0^+$ superallowed nuclear β transitions according to

$$|V_{ud}|^2 = \frac{K}{2G_F^2(1 + \Delta)} \cdot \frac{1}{Ft}, \quad 12.$$

where $K = 8,120.2776(9) \times 10^{-10} \text{ GeV}^{-4} \text{ s}$, Δ is the transition-independent correction factor, G_F is the weak interaction constant for purely leptonic muon decay, and Ft is the corrected strength of the transition (Ft value). According to the conserved vector current hypothesis, Ft values of superallowed nuclear β transitions are the same. The Ft value is a function of several transition parameters and, in particular, of the total transition energy, the Q value, provided by Penning-trap mass spectrometry. Because the Ft value is a function of the Q value to the fifth power, the Q values of relevant transitions have to be determined with sub-keV uncertainties. In addition, superallowed nuclear β transitions have a typical decay time of less than 1 s, requiring the use of online facilities. Nineteen superallowed nuclear β transitions have already been addressed by Penning-trap facilities (101), predominantly by JYFLTRAP (Figure 9) (12).

Figure 10 presents the 14 most precise Ft values. The averaged Ft value of $3,072.27(72)$ s results in $|V_{ud}| = 0.97417(21)$. Together with V_{us} and V_{ub} , obtained from investigations of K and B decays, this yields for $\sum_j |V_{uj}|^2$ a value of $0.99978(55)$. Thus, the unitarity of the CKM matrix has been tested at the 0.06% level, demonstrating remarkable agreement with the SM predictions.

5.3. Masses of the Lightest Particles

The properties of the basic building blocks of matter (i.e., the proton, neutron, and electron) provide a network of fundamental parameters that are essential for a detailed and precise understanding of nature and its symmetries. The masses of these three particles, which enter other fundamental constants such as the Rydberg constant or the fine-structure constant α , are of

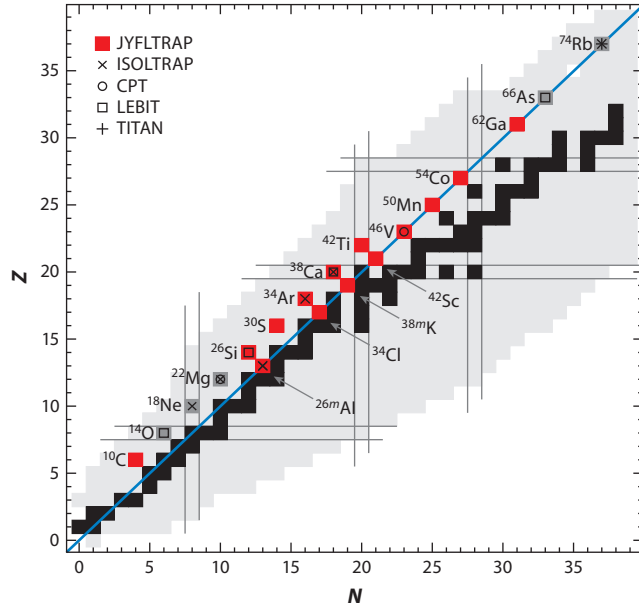


Figure 9

Superallowed nuclear β transitions addressed by Penning-trap facilities until the present (101). Adapted with permission from Reference 115.

particular interest because their present best values at the uncertainty level of $\delta m/m = 10^{-10}$ or below have all been obtained by Penning-trap mass spectrometry, indirectly in the case of the electron and the neutron. A comparison of the masses of the particles and their antiparticles also enables a stringent test of CPT invariance in the leptonic and baryonic sectors. The atomic mass of the proton was recently measured with a purpose-built Penning-trap system with a precision of

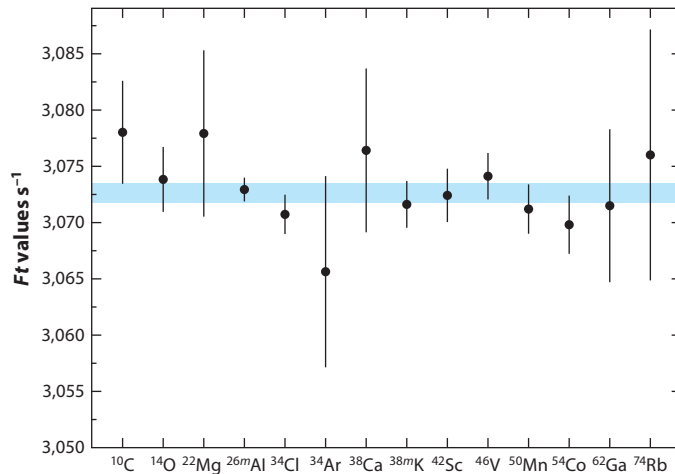


Figure 10

The 14 most precise Ft values of superallowed nuclear β transitions addressed by Penning-trap facilities (186). The blue band represents the mean Ft value and its uncertainty.

32 ppt by use of $^{12}\text{C}^{6+}$ as mass reference (97). However, this experiment found a not-yet-understood shift of approximately 3σ compared with the CODATA2014 (187) value, based on two older Penning-trap mass measurements (188, 189).

The neutron mass was extracted from direct Penning-trap mass measurements of the proton and deuteron masses and the deuteron binding energy on the basis of an absolute wavelength determination of the 2.2-MeV np capture γ -ray (190, 191). By combining the most accurate Penning-trap measurement of the magnetic moment of a single electron bound to a carbon nucleus at the 3×10^{-11} level with a state-of-the-art calculation in the framework of bound-state quantum electrodynamics, the CODATA2014 value of the electron mass could be improved by a factor of 13 (192, 193). Using this value and the proton mass result, one can determine the proton-to-electron mass ratio with a relative precision of 43 ppt. This is an improvement by a factor of two compared with the previous best value (187).

5.3.1. Fundamental symmetry tests in nuclear physics. Atomic mass models play a crucial role in predicting the masses of exotic nuclei relevant to both nuclear structure and nuclear astrophysics. Often, the hundreds-of-keV uncertainty in the prediction from global mass models or the extrapolation of the mass surface of the atomic mass evaluation is sufficient. However, in some cases, such as in predictions of atomic masses relevant for the rp-process or in searches for proton-radioactivity candidates, more precise and accurate predictions are required. The isobaric multiplet mass equation (IMME) is a commonly used local mass model that has been particularly successful. The IMME relates isobaric analog states (IAS), which are states found in different isobars that shares the same nuclear spin, parity, and isospin T but have a different isospin projection T_z . The degeneracy of these IAS is broken in the nucleus because of the electromagnetic interaction and the mass difference between the up and down quarks. This results in a variation of the mass excess (ME) of IAS that follows quadratic behavior with the isospin projection $T_z = (N - Z)/2$ described by the IMME:

$$\text{ME}(A, T, T_z) = a(A, T) + b(A, T)T_z + c(A, T)T_z^2, \quad 13.$$

where a , b , and c are coefficients typically fitted from known MEs that depend on all quantum numbers except T_z .

Because of its common use as a local mass formula, the IMME has been scrutinized and tested for its accuracy. Penning-trap mass spectrometry has played an important role in this endeavor. Indeed, mass measurements of the $A = 9$ quartet using TITAN, coupled with shell model calculations, have elucidated the nature of the breakdown of the IMME in this quartet (194). Furthermore, deviations have been found in $A = 21$ using TITAN (195), $A = 31$ using JYFLTRAP (153), $A = 32$ using LEBIT (196), and $A = 35$ using ISOLTRAP (197). Recently, a novel method was proposed to probe for potential cubic terms in the IMME; with this method, a large cubic term was found for the $A = 29$, $T = 5/2$ multiplet (198).

6. CONCLUSION AND OUTLOOK

From the very early days, when atomic mass spectrometry was used to identify isotopes as parts of the same chemical element with different numbers of neutrons, to today, when specialized and highly developed mass measurement systems are being employed with increasing sensitivity and resolution, Penning-trap mass spectrometry has played a major role in many sectors of atomic and nuclear physics. Mass measurements of stable and unstable atoms and isotopes provide significant input to many outstanding investigations in nuclear physics encompassing all aspects of the field. Penning-trap mass measurement technology is currently the leading approach for these

investigations because it provides very well controlled measurement systems and methods based on ToF, frequency, or even charged-particle rotational-motion frequency modulation (phase shift). The method is mature, reliable, and systematically reproducible; moreover, it can be coupled to accelerator systems and used at very high speed, matched to the lifetime of the isotopes. The Penning-trap methods are evolving to provide better and better data, and they can be coupled to or complemented by other ion traps, such as preparation systems and cleaning systems like MR-ToF.

In the future, Penning traps will be more and more widely used to carry out mass spectrometry at ever-increasing precision and resolution. Virtually all accelerator facilities for isotopes will have (or already have) Penning traps installed and will use them for mass determinations or preparation of beams for additional and complementary spectroscopy. The field of Penning-trap spectroscopy in nuclear physics at accelerators started in the late 1980s and is still growing, developing new aspects and applications, with ever greater impact and reach. While the method has now been fully accepted by the community for mass measurements, future developments will focus on improved sensitivity, in terms of both selecting the species of interest among many coproduced contaminants and carrying out mass determinations at very low production rates. Penning-trap mass spectrometry will continue to play a major role in atomic and nuclear physics in the coming decade.

DISCLOSURE STATEMENT

The authors are not aware of any affiliations, memberships, funding, or financial holdings that might be perceived as affecting the objectivity of this review.

ACKNOWLEDGMENTS

J.D. appreciates and acknowledges support from the Natural Sciences and Engineering Research Council of Canada and the National Research Council. S.E. and K.B. acknowledge support from the Max Planck Society. M.B. acknowledges support from the National Science Foundation under grant number PHY-1713857.

LITERATURE CITED

1. Thomson JJ. *Proc. R. Soc. A* 89:1 (1913)
2. Audi G. *Int. J. Mass Spectrom.* 251:85 (2006)
3. Myers EG, et al. *Phys. Rev. Lett.* 114:013003 (2015)
4. Eliseev S, et al. *Phys. Rev. Lett.* 115:062501 (2015)
5. Rainville S, et al. *Science* 303:334 (2004)
6. Brown LS, Gabrielse G. *Rev. Mod. Phys.* 58:233 (1986)
7. Brown LS, Gabrielse G. *Phys. Rev. B* 25:2423(R) (1982)
8. Gabrielse G. *Int. J. Mass Spectrom.* 279:107 (2009)
9. Block M, et al. *Eur. Phys. J. D* 45:39 (2007)
10. Block M, et al. *Nucl. Phys. A* 944:471 (2015)
11. Ketelaer J, et al. *Nucl. Instrum. Methods A* 594:162 (2008)
12. Szerypo J, et al. *Nucl. Phys. A* 701:588 (2002)
13. Mukherjee M, et al. *Eur. Phys. J. A* 35:1 (2008)
14. Ringle R, Schwarz S, Bollen G. *Int. J. Mass Spectrom.* 349:87 (2013)
15. Dilling J, et al. *Int. J. Mass Spectrom.* 251:198 (2006)
16. Clark J, et al. *Nucl. Instrum. Methods B* 204:487 (2003)

17. Mount B, Redshaw M, Myers E. *Hyperfine Interact.* 199:327 (2011)
18. Diehl C, et al. *Hyperfine Interact.* 199:291 (2011)
19. Repp J, et al. *Appl. Phys. B* 107:983 (2012)
20. Roux C, et al. *Appl. Phys. B* 107:997 (2012)
21. Redshaw M, et al. *Nucl. Instrum. Methods B* 376:302 (2016)
22. Gräff G, Kalinowsky H, Traut J. *Z. Phys. A* 297:35 (1980)
23. Eliseev S, et al. *Phys. Rev. Lett.* 110:082501 (2013)
24. Comisarow MB, Marshall AG. *Chem. Phys. Lett.* 25:282 (1974)
25. König M, et al. *Int. J. Mass Spectrom.* 142:95 (1995)
26. Bollen G, et al. *Nucl. Instrum. Methods B* 70:490 (1992)
27. Kretzschmar M. *Int. J. Mass Spectrom.* 264:122 (2007)
28. George S, et al. *Int. J. Mass Spectrom.* 264:110 (2007)
29. George S, et al. *Phys. Rev. Lett.* 98:162501 (2007)
30. Ringle R, et al. *Int. J. Mass Spectrom.* 262:33 (2007)
31. Eliseev S, et al. *Int. J. Mass Spectrom.* 262:45 (2007)
32. Eliseev S, et al. *Phys. Rev. Lett.* 107:152501 (2011)
33. Eliseev S, et al. *Appl. Phys. B* 114:107 (2014)
34. Wineland DJ, Dehmelt HG. *J. Appl. Phys.* 46:919 (1975)
35. Cornell EA, et al. *Phys. Rev. A* 41:312 (1990)
36. Verdu J, et al. *Phys. Scr.* T112:68 (2004)
37. Cornell EA, et al. *Phys. Rev. Lett.* 63:1674 (1989)
38. Sturm S, Wagner A, Schabinger B, Blaum K. *Phys. Rev. Lett.* 107:143003 (2011)
39. Gärtner G, Klempt E. *Z. Phys. A* 287:1 (1976)
40. Dehmelt H. *Adv. At. Mol. Phys.* 3:53 (1967)
41. Farnham DL, Van Dyck RS, Schwinberg PB. *Phys. Rev. Lett.* 75:3598 (1995)
42. Gabrielse G, et al. *Phys. Rev. Lett.* 66:1317 (1990)
43. Bollen G, et al. *Hyperfine Interact.* 38:793 (1987)
44. Blumenfeld Y, et al. *Phys. Scr.* T152:014023 (2013)
45. Savard G, et al. *Nucl. Instrum. Methods B* 266:4086 (2008)
46. Geissel H, et al. *Nucl. Instrum. Methods B* 70:286 (1992)
47. Kubo T. *Nucl. Instrum. Methods B* 204:97 (2003)
48. Morrissey D, et al. *Nucl. Instrum. Methods B* 204:90 (2003)
49. Winkler M, et al. *Nucl. Instrum. Methods B* 266:4183 (2008)
50. Hausmann M, et al. *Nucl. Instrum. Methods B* 317:349 (2013)
51. Hofmann S, Münzenberg G. *Rev. Mod. Phys.* 72:733 (2000)
52. Harss B, et al. *Rev. Sci. Instrum.* 71:280 (2000)
53. Wiedenhöver I, et al. In *Proceedings of the 5th International Conference on Fission and Properties of Neutron-Rich Nuclei (ICNF5)*, ed. JH Hamilton, AV Ramayya, p. 144. Singapore: World Sci. (2014)
54. Becchetti F, et al. *Nucl. Instrum. Methods A* 505:377 (2003)
55. Schnatz H, et al. *Nucl. Instrum. Methods A* 251:17 (1986)
56. Stolzenberg H, et al. *Phys. Rev. Lett.* 65:3104 (1990)
57. Moore RB, Rouleau G. *J. Mod. Opt.* 39:361 (1992)
58. Herfurth F, et al. *Nucl. Instrum. Methods A* 469:254 (2001)
59. Lunney D. *J. Phys. G* 44:064008 (2017)
60. Kreim S, et al. *Nucl. Instrum. Methods B* 317:492 (2013)
61. Wolf RN, et al. *Int. J. Mass. Spectrom.* 349:123 (2013)
62. Raimbault-Hartmann H, et al. *Nucl. Instrum. Methods B* 126:378 (1997)
63. Bollen G, et al. *Nucl. Instrum. Methods A* 368:675 (1996)
64. Kellerbauer A, et al. *Phys. Rev. Lett.* 93:072502 (2004)
65. Blaum K, et al. *Eur. Phys. J. A* 15:245 (2002)
66. Elomaa V-V, et al. *Nucl. Instrum. Methods B* 266:4425 (2008)
67. Smorra C, et al. *J. Phys. B* 42:154028 (2009)
68. Chaudhuri A. *Eur. Phys. J. D* 45:47 (2009)

69. Dilling J, et al. *Nucl. Instrum. Methods B* 204:492 (2003)
70. Dombbsky M, et al. *Nucl. Phys. A* 701:486 (2002)
71. Baartman R. *Hyperfine Interact.* 225:69 (2014)
72. Brunner T, et al. *Nucl. Instrum. Methods A* 676:32 (2012)
73. Brodeur M, et al. *Int. J. Mass Spectrom.* 310:20 (2012)
74. Smith M, et al. *Phys. Rev. Lett.* 101:202501 (2008)
75. Lascar D, et al. *Nucl. Instrum. Methods B* 376:262 (2016)
76. Leistenschneider E, et al. arXiv:1710.08537 [nucl-ex] (2017)
77. Lapierre A, et al. *Nucl. Instrum. Methods A* 624:54 (2010)
78. Schultz BE, et al. *Phys. Scr.* T156:014097 (2013)
79. Ettenauer S, et al. *Int. J. Mass Spectrom.* 349:74 (2013)
80. Ettenauer S, et al. *Phys. Rev. Lett.* 107:272501 (2011)
81. Klawitter R, et al. *Phys. Rev. C* 93:045807 (2016)
82. Lascar D, et al. *Phys. Rev. C* 96:044323 (2017)
83. Frekers D, et al. *Phys. Lett. B* 722:233 (2013)
84. Sharma KS, et al. *AIP Conf. Proc.* 455:130 (1998)
85. Block M, et al. *Eur. Phys. J. A* 25:49 (2005)
86. Marx G, et al. *Hyperfine Interact.* 132:463 (2001)
87. Bollen G, et al. *Phys. Rev. Lett.* 96:152501 (2006)
88. Schwarz S, et al. *Nucl. Instrum. Methods B* 204:507 (2003)
89. Savard G, et al. *Nucl. Phys. A* 626:353c (1997)
90. Jokinen A, et al. *Nucl. Phys. A* 746:277c (2004)
91. Ketelaer J, et al. *Phys. Rev. C* 84:014311 (2011)
92. Eibach M, et al. *Phys. Rev. C* 89:064318 (2014)
93. Savard G, Levand AF, Zabransky BJ. *Nucl. Instrum. Methods B* 376:246 (2016)
94. Hirsh TY, et al. *Nucl. Instrum. Methods B* 376:229 (2016)
95. Van Schelt J, et al. *Phys. Rev. Lett.* 111:061102 (2013)
96. Bergström I, et al. *Nucl. Instrum. Methods A* 487:618 (2002)
97. Heiße F, et al. *Phys. Rev. Lett.* 119:033001 (2017)
98. Gastaldo L, et al. *J. Low Temp. Phys.* 176:876 (2014)
99. Crespo JR, et al. *Rev. Sci. Instrum.* 75:1560 (2004)
100. Wang M, et al. *Chin. Phys. C* 41:030003 (2017)
101. Huang WG, et al. *Chin. Phys. C* 41:030002 (2017)
102. Lunney D, Pearson JM, Thibault C. *Rev. Mod. Phys.* 75:1021 (2003)
103. Thibault C, et al. *Phys. Rev. C* 12:644 (1975)
104. Honma M, Otsuka T, Brown BA, Mizusaki T. *Phys. Rev. C* 69:034335 (2004)
105. Lapierre A, et al. *Phys. Rev. C* 85:024317 (2012)
106. Gallant AT, et al. *Phys. Rev. Lett.* 109:032506 (2012)
107. Weinholtz F, et al. *Nature* 498:346 (2013)
108. Rosenbusch M, et al. *Phys. Rev. Lett.* 114:202501 (2015)
109. Hager U, et al. *Phys. Rev. Lett.* 96:043504 (2006)
110. Hager U, et al. *Phys. Rev. C* 75:064302 (2007)
111. Hager U, et al. *Nucl. Phys. A* 793:20 (2007)
112. Hakala J, et al. *Eur. Phys. J. A* 47:129 (2011)
113. Brodeur M, et al. *Hyperfine Interact.* 199:167 (2011)
114. Riisager K. *Phys. Scr.* T152:014001 (2013)
115. Blaum K, Dilling J, Nörtershäuser W. *Phys. Scr.* T152:014017 (2013)
116. Brodeur M, et al. *Phys. Rev. Lett.* 108:052504 (2012)
117. Ryjgov VL, et al. *Phys. Rev. Lett.* 101:012501 (2008)
118. Ringle R, et al. *Phys. Lett. B* 675:170 (2009)
119. Chaudhuri A, et al. *Appl. Phys. B* 114:99 (2014)
120. Geithner W, et al. *Phys. Rev. Lett.* 101:252502 (2008)
121. Block M, et al. *Nature* 463:785 (2010)

122. Minaya Ramirez E, et al. *Science* 337:1207 (2012)
123. Langanke K, Schatz H. *Phys. Scr.* T152:014011 (2013)
124. Schatz H. *Int. J. Mass Spectrom.* 251:293 (2006)
125. Mumpower MR, Surman R, McLaughlin GC, Aprahamian A. *Prog. Part. Nucl. Phys.* 86:86 (2016)
126. Burbidge EM, Burbidge GR, Fowler WA, Hoyle F. *Rev. Mod. Phys.* 29:547 (1957)
127. Arnould M, Gorieli S, Takahashi K. *Phys. Rep.* 450:97 (2007)
128. Arcones A, Thielemann F-K. *J. Phys. G* 40:013201 (2013)
129. Thielemann F-K, Eichler M, Panov IV, Wehmeyer B. *Annu. Rev. Nucl. Part. Sci.* 67:253 (2017)
130. Abbott BP, et al. *Phys. Rev. Lett.* 119:161101 (2017)
131. Arcavi I, et al. *Nature* 551:64 (2017)
132. Kasen D, et al. *Nature* 551:80 (2017)
133. Brett S, et al. *Eur. Phys. J. A* 48:184 (2012)
134. Simon VV, et al. *Phys. Rev. C* 85:064308 (2012)
135. Manea V, et al. *Phys. Rev. C* 88:054322 (2013)
136. de Roubin A, et al. *Phys. Rev. C* 96:014310 (2017)
137. Atanasov D, et al. *Phys. Rev. Lett.* 115:232501 (2015)
138. Van Schelt J, et al. *Phys. Rev. C* 85:045805 (2012)
139. Kankainen A, et al. *J. Phys. G* 39:093101 (2012)
140. Woosley SE, Taam RE. *Nature* 263:101 (1976)
141. Wallace RK, Woosley SE. *Astrophys. J. Suppl. Ser.* 45:389 (1981)
142. Schatz H, et al. *Phys. Rev. Lett.* 86:471 (2001)
143. Clark JA, et al. *Phys. Rev. C* 75:032801(R) (2007)
144. Fallis J, et al. *Phys. Rev. C* 78:022801(R) (2008)
145. Schury P, et al. *Phys. Rev. C* 75:055801 (2007)
146. Savory J, et al. *Phys. Rev. Lett.* 102:132501 (2009)
147. Herfurth F, et al. *Eur. Phys. J. A* 47:75 (2011)
148. Martin A, et al. *Eur. Phys. J. A* 34:341 (2007)
149. Haettner E, et al. *Phys. Rev. Lett.* 106:122501 (2011)
150. Kankainen A, et al. *Phys. Rev. C* 82:034311 (2010)
151. Elomaa V-V, et al. *Phys. Rev. Lett.* 102:252501 (2009)
152. Weber C, et al. *Phys. Rev. C* 78:054310 (2008)
153. Kankainen A, et al. *Phys. Rev. C* 93:041304(R) (2016)
154. Nesterenko DA, et al. *J. Phys. G* 44:065103 (2017)
155. Canete L, et al. *Eur. Phys. J. A* 52:124 (2016)
156. Pauli W. *Open letter to the group of radioactive people at the Gauverein meeting in Tübingen.* <http://microboone-docdb.fnal.gov/cgi-bin/RetrieveFile?docid=953;filename=pauli%20letter1930.pdf> (in German) (1930)
157. Cowan CL, et al. *Science* 124:103 (1956)
158. Fukuda Y, et al. *Phys. Rev. Lett.* 81:1562 (1998)
159. Abazajian KN, et al. arXiv:1204.5379 [hep-ph] (2012)
160. Adhikari R, et al. arXiv:1602.04816v2 [hep-ph] (2017)
161. Drexlin G, et al. *Adv. High Energy Phys.* 293986 (2013)
162. Avignone FT III, et al. *Rev. Mod. Phys.* 80:481 (2008)
163. Bernabeu G, Rujula A, Jarlskog C. *Nucl. Phys. B* 223:15 (1983)
164. Barabash AS. arXiv:1702.06340v1 [nucl-ex] (2017)
165. Redshaw M, et al. *Phys. Rev. Lett.* 98:053003 (2007)
166. Douysset G, et al. *Phys. Rev. Lett.* 86:4259 (2001)
167. Redshaw M, et al. *Phys. Rev. Lett.* 102:212502 (2009)
168. Rahaman S, et al. *Phys. Lett. B* 662:111 (2008)
169. Lincoln DL, et al. *Phys. Rev. Lett.* 110:012501 (2013)
170. Rahaman S, et al. *Phys. Lett. B* 703:412 (2011)
171. Bustabad S, et al. *Phys. Rev. C* 88:022501(R) (2013)
172. Kolhinen VS, et al. *Phys. Rev. C* 82:022501(R) (2010)

173. Alanssari M, et al. *Phys. Rev. Lett.* 116:072501 (2016)
174. Eliseev SA, Novikov YN, Blaum K. *J. Phys. G* 39:124003 (2012)
175. Eibach M, et al. *Phys. Rev. C* 94:015502 (2016)
176. Eliseev S, et al. *Phys. Rev. Lett.* 106:052504 (2011)
177. Eliseev S, et al. *Phys. Rev. C* 84:012501(R) (2011)
178. Kraus C, et al. *Eur. Phys. J. C* 40:447 (2005)
179. Weinheimer C. *Prog. Part. Nucl. Phys.* 57:22 (2006)
180. Aseev N, et al. *Phys. Rev. D* 84:112003 (2011)
181. KATRIN Collab. Design rep. FZKA 7090, Karlsruhe Inst. Technol., Karlsruhe, Ger. <https://publikationen.bibliothek.kit.edu/270060419> (2004)
182. Gastaldo L, et al. *Eur. Phys. J. Spec. Top.* 226:1623 (2017)
183. Alpert B, et al. *Eur. Phys. J. C* 75:112 (2015)
184. Streubel S, et al. *Appl. Phys. B* 114:137 (2014)
185. Esfahani AA, et al. *J. Phys. G* 44:054004 (2017)
186. Hardy JC, Towner IS. *Phys. Rev. C* 91:025501 (2015)
187. Mohr PJ, et al. *Rev. Mod. Phys.* 88:035009 (2016)
188. Van Dyck RS, et al. *AIP Conf. Proc.* 457:101 (1999)
189. Solders A, et al. *Phys. Rev. A* 78:012514 (2008)
190. Greene GL, et al. *Phys. Rev. Lett.* 56:819 (1986)
191. Zafonte SL, Van Dyck RS Jr. *Metrologia* 52:280 (2015)
192. Sturm S, et al. *Nature* 506:467 (2014)
193. Köhler F, et al. *J. Phys. B* 48:144032 (2015)
194. Brodeur M, et al. *Phys. Rev. Lett.* 108:212501 (2012)
195. Gallant AT, et al. *Phys. Rev. Lett.* 113:082501 (2014)
196. Kwiatkowski AA, et al. *Phys. Rev. C* 80:051302 (2009)
197. Yazidjian C, et al. *Phys. Rev. C* 76:024308 (2007)
198. Brodeur M, et al. *Phys. Rev. C* 96:034316 (2017)